INTERNATIONAL JOURNAL FOR NUMERICAL METHODS IN FLUIDS
Int. J. Numer. Meth. Fluids 2000; **33**: 833–846

A modified finite element method for determining equilibrium capillary surfaces of liquids with specified volumes

Nicholas J. Nigro[a,*], Benjamin P. Zellmer[a], Dongkai Shangguan[b] and Ping S. Lee[c]

[a] *Department of Mechanical and Industrial Engineering, Marquette University, Milwaukee, WI, U.S.A.*
[b] *Weston Automotive Systems, Ford Motor Company, Dearborn, MI, U.S.A.*
[c] *Advanced Technology Milwaukee Laboratory, Rockwell Automation, Milwaukee, WI, U.S.A.*

SUMMARY

This paper describes a modified finite element method (MFEM) for determining the static equilibrium shape of the capillary surface of a liquid with a prescribed volume constrained by rigid boundaries with arbitrary shapes. It is assumed that the liquid is in static equilibrium under the influence of surface tension, adhesion, and gravity forces. This problem can be solved by employing the conventional FEM; however, a major difficulty arises due to the presence of the volume (integral) constraint and usually requires the use of the Lagrange multiplier method, the sequential unconstrained minimization technique, or the augmented Lagrange multiplier method. With the MFEM, the space variables defining the equilibrium surfaces (or curves) are expanded in terms of parametric interpolation functions, which are designed such that the boundary conditions *and the integral constraint equation* are automatically satisfied during each iteration of a direct numerical search process. Hence, there is no need to include Lagrange multipliers and/or penalty factors and the problem can be treated more simply as one involving unconstrained optimization. This investigation indicates that the MFEM is more efficient and reliable than the other methods. Results are presented for several case study problems involving liquid solder drops. Copyright © 2000 John Wiley & Sons, Ltd.

KEY WORDS: capillary surface; modified finite element method; rigid boundary

1. INTRODUCTION

This paper describes a modified finite element method (MFEM) for determining the equilibrium shape of the capillary surface of a liquid with specified volume, which is constrained by rigid, arbitrary boundaries. It is assumed that the liquid is in static equilibrium under the influence of surface tension, adhesion, and gravity forces. The theory and mathematical models governing this problem are discussed by Laplace [1], Concus and Finn [2], and Finn [3]. The

* Correspondence to: Department of Mechanical and Industrial Engineering, Marquette University, Haggerty Engineering Hall 239, PO Box 1881, Milwaukee, WI 52233, U.S.A.

Received September 1998
Revised February 1999

first investigators [4–6] who obtained numerical results for this problem employed finite difference and variational methods. Hinata *et al.* [7] and Wagner [8] were the first investigators to apply the FEM to this problem. They utilized triangular elements and linear interpolation functions to solve the Plateau problem, which does not involve a volume constraint. Horning and Mittlemann [9] extended this by employing the use of the Lagrange multiplier method to determine the equilibrium shapes of capillary surfaces of liquids with specified volumes, which are bounded by vertical and horizontal (plane) surfaces. However, they avoided the difficulty of including the integral constraint equation in their formulation by assigning an arbitrary value to the multiplier, solving this problem, and then determining the corresponding volume.

Several investigators [10–13] have applied the FEM to determine the equilibrium shapes of solder joints (with prescribed volumes) formed in an oven during a reflow process by assuming that the final (solidified) form of the joint is identical to the static equilibrium shape of the liquid solder. Nigro *et al.* [12,13] presented a parametric form of the FEM, which proved to be efficient for those solder joint formation problems where the boundary conditions included prescribed derivatives (i.e., contact angles) of the spatial co-ordinates and/or where the location of the boundary was not known *a priori* (i.e., infinite wetting problem).

A major difficulty in the solution of this problem by the FEM stems from the presence of the volume (integral) constraint. The solution is normally obtained by employing the use of the Lagrange multiplier method (LM), the sequential unconstrained minimization technique (SUMT), or the augmented Lagrange multiplier method (ALM). All of these methods [14] require the user to modify the original performance index (potential energy) with an additional term (integral constraint), which is multiplied by a Lagrange multiplier or a penalty factor, or both. The resulting problem is then solved by an iterative process until the constraint condition is satisfied. This process increases the solution time and, more importantly, in the case of the SUMT and the ALM, requires experience and/or insight in order to select appropriate values for the penalty factor.

The purpose of this paper is to present an MFEM in which the space variables defining the fluid equilibrium surfaces (or curves) are expanded in terms of parametric interpolation functions, which are designed such that all of the boundary conditions *and the integral constraint equation* are automatically satisfied during every iteration of a direct numerical optimization search process. Hence, there is no need to include the use of a Lagrange multiplier and/or penalty factor and the problem can be treated more simply as one involving unconstrained optimization.

2. THEORY

The variational problem for determining the equilibrium shape of the surface of a liquid with a specified volume constrained by rigid boundaries (see Figure 1) is given below

$$\min E_{\mathrm{p}} = E_{\mathrm{s}} + E_{\mathrm{g}} + E_{\mathrm{w}} \tag{1}$$

subject to

$$\int_V \mathrm{d}v = V_0 \tag{2}$$

$$z = f(x, y) \quad or \quad \left.\begin{matrix} z_{,x} = g(x, y) \\ z_{,y} = h(x, y) \end{matrix}\right] \quad \text{on } \Gamma \tag{3}$$

where E_p is potential energy and

$$E_\mathrm{s} = \text{free surface energy} = \int_a \gamma \, \mathrm{d}a \tag{4}$$

$$E_\mathrm{g} = \text{gravitational energy} = \int_V \rho g z \, \mathrm{d}V \tag{5}$$

$$E_\mathrm{w} = \text{wetting energy} = \int_{a^*} -\gamma\beta \, \mathrm{d}a^* \tag{6}$$

where $\beta = \cos(\theta)$; θ is the contact angle; γ is the surface tension constant for the liquid/air interface; ρ is the liquid density; g is the gravitational constant; V_0 is the prescribed volume of liquid; $f(x, y)$, $g(x, y)$, and $h(x, t)$ denote prescribed functions of z, $z_{,x}$, and $z_{,y}$ on Γ; a^* is the wetted area; a is the liquid/air interface area; and Γ is the liquid/air boundary.

The integrals for the gravitational energy and the volume can be transformed to surface integrals by employing Gauss's theorem; this yields

$$\int_v \mathrm{d}v = \int_{a_{xy}} z \, \mathrm{d}x \, \mathrm{d}y \tag{7}$$

and

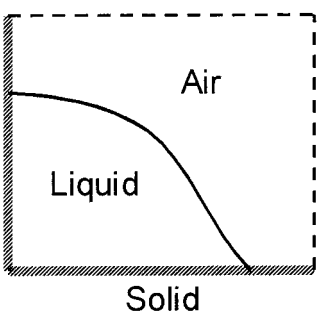

Figure 1. Liquid constrained by rigid boundaries.

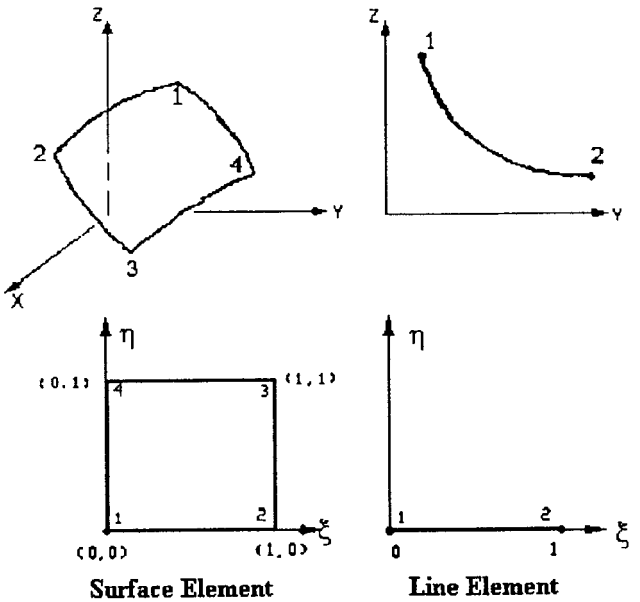

Figure 2. Elements for two- and three-dimensional boundaries.

$$E_g = \int_{a_{xy}} \frac{1}{2} \rho g z^2 \, dx \, dy \tag{8}$$

where a_{xy} is the projection of a on the xy-plane.

In this study, the liquid capillary and boundary surfaces for a three-dimensional problem are discretized with the use of four-node curvilinear quadrilateral elements, while, for a planar problem, the boundary curves are discretized with the use of curved line elements as shown below in Figure 2.

The spatial co-ordinates are expanded (over each finite element) in terms of the element nodal co-ordinates and parametric interpolation functions as defined below

$$\bar{r}^e = (x^e, y^e, z^e), \qquad \bar{r}_0^e = (x_0^e, y_0^e, z_0^e) \tag{9}$$

where $x^e = x_0^e$, $y^e = y_0^e$, and $z^e = z_0^e(1 + c\delta)$

$$\begin{aligned} \bar{r}_0^e = {} & \phi_1 \bar{r}_{00}^e + \phi_2 \bar{r}_{01}^e + \phi_3 \bar{r}_{10}^e + \phi_4 \bar{r}_{11}^e + \phi_5 \bar{r}_{00,\xi}^e + \phi_6 \bar{r}_{01,\xi}^e + \phi_7 \bar{r}_{10,\xi}^e + \phi_8 \bar{r}_{11,\xi}^e + \phi_9 \bar{r}_{00,\eta}^e \\ & + \phi_{10} \bar{r}_{01,\eta}^e + \phi_{11} \bar{r}_{10,\eta}^e + \phi_{12} \bar{r}_{11,\eta}^e \end{aligned} \tag{10}$$

where $\bar{r}^e = \bar{r}^e(\xi, \eta)$, $\bar{r}_{00}^e = \bar{r}^e(0, 0)$, $\bar{r}_{01}^e = \bar{r}^e(0, 1)$, $\bar{r}_{10}^e = \bar{r}^e(1,0)$, $\bar{r}_{11}^e = \bar{r}^e(1, 1)$, $\bar{r}_{\xi\eta,\xi}^e$ is the derivative of $\bar{r}^e$ with respect to ξ, $\bar{r}_{\xi\eta,\eta}^e$ is the derivative of $\bar{r}^e$ with respect to η, $\bar{r}_{00,\xi}^e = \bar{r}_{,\xi}^e(0, 0)$, etc., c is a constant, ϕ_i are cubic interpolation functions of ξ and η (see Appendix B), and

$$\delta(\xi, \eta) = \xi^2(1-\xi)^2 + \eta^2(1-\eta)^2 + \xi\eta(1-\xi)(1-\eta) \tag{11}$$

The prescribed boundary conditions are satisfied by assigning appropriate values to the corresponding nodal co-ordinates that lie on that boundary. The remaining nodal co-ordinates are retained as unknowns to be determined in the optimization process. In this study, the spatial co-ordinate z_0 was modified by multiplying it by the factor $(1 + c\delta)$; this results in interpolation functions that are of higher order than those used to approximate the x and y spatial variables. The interpolation function (δ) is designed such that the conditions $\bar{r} = \bar{r}_0$, $\bar{r}_{,\xi} = \bar{r}_{0,\xi}$, and $\bar{r}_{,\eta} = \bar{r}_{0,\eta}$ are automatically satisfied (regardless of the value of c) at all of the element nodes for every set of nodal co-ordinates selected by the direct search algorithm. As a special case, the planar problem requires only one parameter (ξ); hence the corresponding forms and equations can be obtained by setting one of the parameters (e.g., η) equal to zero.

The total potential energy for the problem is obtained in parametric form by summing the contributions for each element as follows:

$$E_{\mathrm{p}} = \sum_{e=1}^{m} (E_{\mathrm{s}}^{(e)} + E_{\mathrm{g}}^{(e)}) + \sum_{e=1}^{m^*} E_{\mathrm{w}}^{(e)} \tag{12}$$

$$E_{\mathrm{s}}^{(e)} = \int_0^1 \int_0^1 \gamma(\tilde{E}\tilde{G} - \tilde{F}^2)\, \mathrm{d}\xi\, \mathrm{d}\eta \tag{13}$$

$$E_{\mathrm{g}}^{(e)} = \int_0^1 \int_0^1 \frac{1}{2} J^{(e)} \rho g (z^{(e)})^2\, \mathrm{d}\xi\, \mathrm{d}\eta \tag{14}$$

$$E_{\mathrm{w}}^{(e)} = \int_0^1 \int_0^1 -\gamma J^{(e)} \beta\, \mathrm{d}\xi\, \mathrm{d}\eta \tag{15}$$

$$V = \sum_{e=1}^{m} \int_0^1 \int_0^1 z^{(e)} J^{(e)}\, \mathrm{d}\xi\, \mathrm{d}\eta \tag{16}$$

where

$$J^{(e)} = \text{Jacobian} = \begin{vmatrix} x_{,\xi}^e & x_{,\eta}^e \\ y_{,\xi}^e & y_{,\eta}^e \end{vmatrix} \tag{17}$$

$$\begin{aligned} \tilde{E} &= (x_{,\xi})^2 + (y_{,\xi})^2 + (z_{,\xi})^2 \\ \tilde{F} &= x_{,\xi}x_{,\eta} + y_{,\xi}y_{,\eta} + z_{,\xi}z_{,\eta} \\ \tilde{G} &= (x_{,\eta})^2 + (y_{,\eta})^2 + (z_{,\eta})^2 \end{aligned} \tag{18}$$

and m is the number of elements used to define the capillary surface, and m^* is the number of elements used to define the wetted surface.

It should be noted that, if the wetted surface area is assumed to be fixed (e.g., finite wetting problem), then the wetting energy is constant and can be dropped from Equations (1) and (12).

3. NUMERICAL ALGORITHM

The unknown nodal co-ordinates can be determined by employing the LM method and developing the Euler–Lagrange finite element equations. These equations, which include the integral constraint equation and contain an additional unknown Lagrange multiplier, are non-linear and require a numerical method (e.g., Newton–Raphson) for an iterative solution. Instead, in this study, the unknown nodal co-ordinates are determined by direct minimization of the potential energy with the use of a numerical search (Hooke and Jeeves [15]) algorithm. The steps for implementing the solution process in this study are given below.

Step 1. An initial estimate for each of the unknown nodal co-ordinates is specified.

Step 2. The value of c in Equation (9) is determined such that the volume constraint (Equation (2)) is satisfied with these values; this yields

$$c = \frac{V_0 - \sum_{e=1}^{m} \iint z_0^e J^e \, \mathrm{d}\xi \, \mathrm{d}\eta}{\sum_{e=1}^{m} \iint z_0^e \delta J^e \, \mathrm{d}\xi \, \mathrm{d}\eta} \tag{19}$$

As an analogy, the constant c can be viewed as an 'internal pressure' in the liquid, which causes the capillary surface to inflate (or deflate) in order to satisfy the volume constraint. It is important to note that this inflation or deflation is accomplished while maintaining all of the values of the nodal co-ordinates. In those problems involving an integral constraint with a form of integrand that does not permit an explicit solution of the constant c, the value of the constant can be determined by employing an optimization routine (involving a single variable direct search algorithm) to minimize the function Φ, where

$$\Phi = \mathrm{abs}\left(\sum_{e=1}^{m} \iint z_0^e (1 + c\delta) J^e \, \mathrm{d}\xi \, \mathrm{d}\eta - V_0 \right) \tag{20}$$

Step 3. The integral expressions given in Equation (12) are evaluated numerically by employing a nine-point Gauss quadrature algorithm and the value of the potential energy is tested to determine if it corresponds to a local minimum. If not, the values of the unknown global nodal co-ordinates are updated by the Hooke and Jeeves algorithm and Step 2 is repeated.

Step 4. Steps 2 and 3 are repeated until the error criterion for the relative minimum is satisfied.

4. RESULTS

The motivation for developing the MFEM stemmed from the need of manufacturing engineers in the electronic assembly industry to develop methods that would enable them to predict the shapes of solder joints formed in an infrared oven during a solder reflow process. (The volume of the solder joint is determined from the volume of the solder paste.) To date, the vast majority of the methods that have been proposed to solve this problem are based on the assumption that the final shape of the solidified joint is identical to the static equilibrium shape of the melted (liquid) solder. Results obtained under this assumption have proven to be in good agreement with those obtained experimentally. In this investigation, the MFEM was tested by applying it to several case study problems involving both two- and three-dimensional liquid solder drops.

Results were obtained for the shapes of two-dimensional liquid solder drops in a 90° corner formed by the intersection of the xy and xz planes (see Figure 3). The results are based on the following assumptions: (a) the dimension of the drop in the x-direction is very large relative to the y- and z-dimensions; (b) the cross-section of the drop is uniform along the x-direction; and (c) the wetted areas on the vertical and horizontal surfaces are prescribed, i.e., the liquid solder is prevented from spreading beyond the edge points due to the finite tinning.

Figure 4 shows a comparison of two different liquid surface profiles obtained using the MFEM with corresponding profiles obtained from the direct substitution method (DSM). In the DSM one of the dependent nodal co-ordinates is eliminated from the problem by solving it explicitly as a function of the liquid volume and the remaining independent nodal co-ordinates. In general, this method is not feasible for those problems in which the volume integrand is highly non-linear or for finite element solutions involving a large number of elements. The figure shows that the results from the MFEM, which were obtained by discretizing the liquid surface with one element, are indistinguishable from those obtained with the DSM. Moreover, although not shown here, the results compared favorably with experimental values [13].

Figure 5 contains plots showing the variation of the 'pressure parameter' (c) and the total potential energy with increasing number of Hooke and Jeeves searches (iterations) during the solution process for each of the two cases shown in Figure 4. It can be seen that, in general, the pressure parameter converges asymptotically to its final value (approximately zero) simultaneously as the potential energy attains its minimum value.

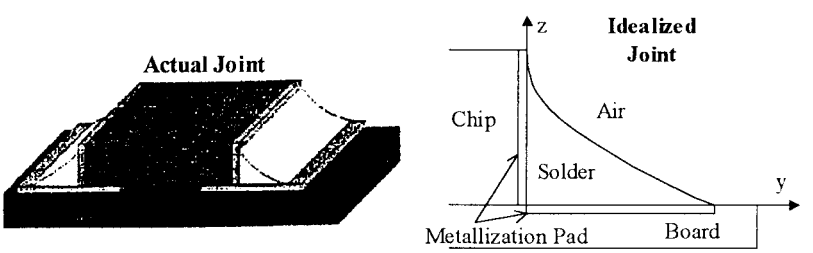

Figure 3. Two-dimensional liquid solder drop.

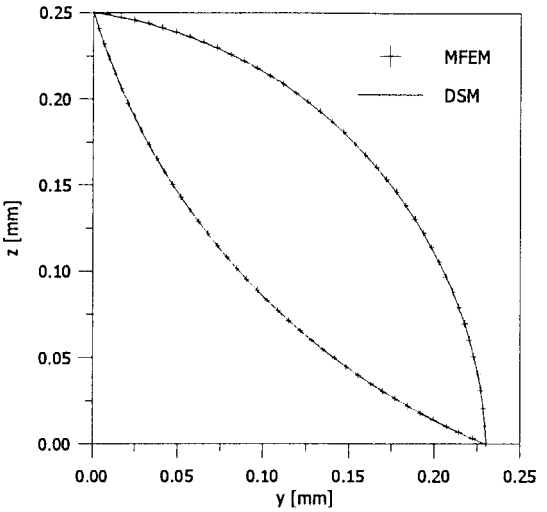

Figure 4. Comparison of two-dimensional liquid profiles; $\gamma = 490$ dyn cm^{-1}, $\rho = 0.00834$ g m^{-3}, $g = 981$ mm s^{-2}.

The MFEM was also employed to predict the shapes of three-dimensional liquid solder drops formed around 'J leads', which rest on a horizontal rectangular pad (see Figure 6). The results are based on the following assumptions: (a) the system (pad, solder drop, lead) is

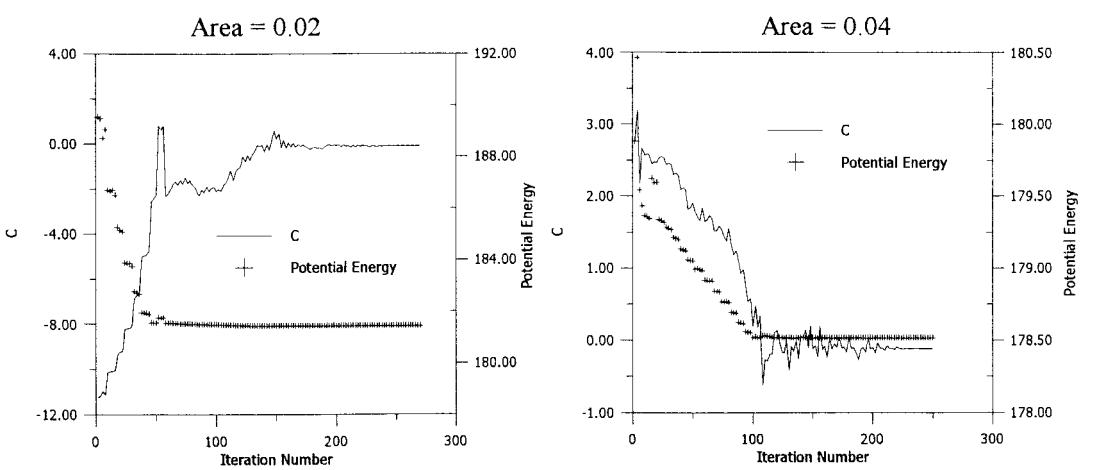

Figure 5. Pressure parameter and potential energy versus number of iterations.

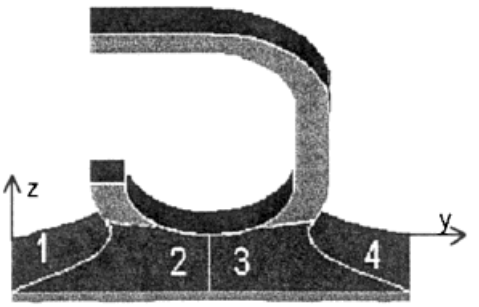

Figure 6. Three-dimensional liquid solder droplet.

symmetric with respect to its centerline *yz* plane; (b) the liquid volume is sufficiently large such that the rectangular pad is completely wetted by the solder drop; (c) the liquid solder is prevented from flowing over the edges of the top surface of the lead; and (d) the lead's front vertical face (parallel to the *yz* plane) and its bottom surface are completely tinned so that the contact angle at every point of the advancing liquid/solid interface on these surfaces is equal to zero. If the solder reaches the front top edge of the lead during the optimization process, then the contact angle at that point is released from its prescribed zero value, treated as an unknown, and determined by the minimization process. The last two assumptions are based on observations of photographs of experimental joints.

All of the results presented in this study were obtained with the MFEM by modeling the liquid surface with four elements (see Figure 6). Plots of a typical front and side view of the

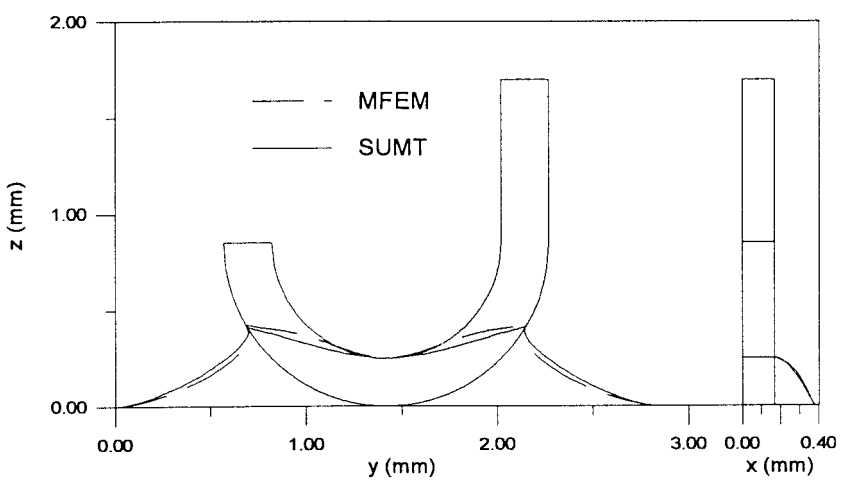

Figure 7. Front and side profiles for three-dimensional joint.

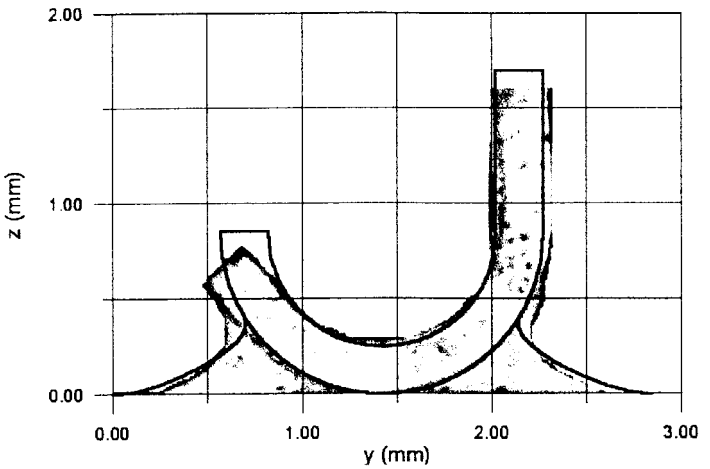

Figure 8. Comparison with experimental results.

system for one of the case studies are shown in Figure 7. It is important to note that the liquid has reached the top edge of the lead at its centerline point. This occurred for all of the cases studied in this investigation.

Several studies were conducted in order to verify the results predicted by the MFEM. Figure 7 shows good agreement between the front and side liquid profiles, which were obtained with both the SUMT and MFEM for one of the cases. As shown in Figure 8, results from the MFEM for the front profile of the liquid also compared favorably with the experimental profile obtained for one of the cases.

Figure 9 contains plots that show the variation of the 'pressure parameter' (c) and the total potential energy with increasing number of Hooke and Jeeves searches (iterations) during the solution process for one of the test cases. It can be seen that, as in the case of the two-dimensional problem, the pressure parameter converges asymptotically to its final value simultaneously as the potential energy attains its minimum value. This behavior was observed in all of the cases that were investigated in this study.

The efficiency of the MFEM was evaluated by comparing the CPU run-times associated with the J lead programs for the MFEM and the SUMT. The results of this comparison appear in Table I. As stated earlier, the MFEM does not require any input from the user other than the system parameters and the initial values for the unknown nodal co-ordinates. However, when using the SUMT, the user must also specify an initial value (estimate) for the penalty factor. After evaluating the results, the user must then modify (update) the value for the penalty factor. This process must be continued until the volume (integral) constraint is satisfied with the smallest possible value of the penalty factor. The results indicate that the average run-time for the SUMT (for a single run) was shorter than that for the MFEM. This is due to the extra calculations associated with the determination of the pressure parameter (c) in the MFEM. However, the total run-time for determining the optimal shape of the solder

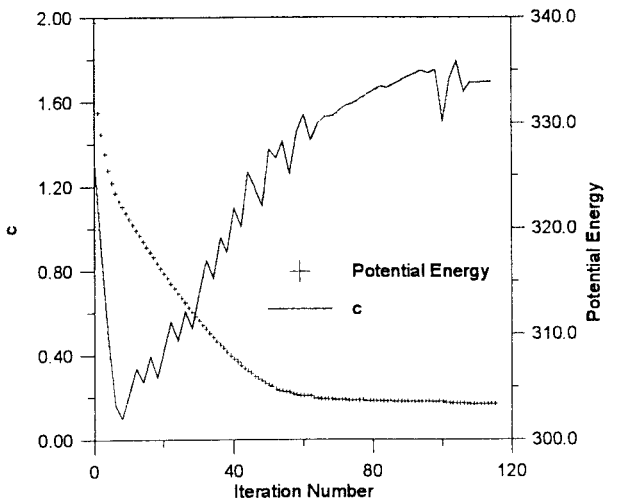

Figure 9. Pressure parameter and potential energy versus number of iterations for the three-dimensional case.

joint is significantly longer for the SUMT, which, for this case, required ten separate runs in order to obtain the minimum penalty factor which satisfied the volume constraint. (It is important to note that this total run-time accounts only for the CPU run-time and does not include the time required to assimilate the results and update the value of the penalty factor.) This proved to be true for all of the test cases studied in this investigation.

Table I. CPU run-time data for MFEM and SUMT.

Run	CPU run-time[a]	
	MFEM (s)	SUMT (s)
1	4.23	2.53
2		2.40
3		3.24
4		6.65
5		4.23
6		3.68
7		3.51
8		4.78
9		3.95
10		3.20
Total	4.23	38.2
Average	4.23	3.82

[a] These results were obtained using a computer with a 350 MHz Pentium II processor.

5. CONCLUSIONS

This paper describes an MFEM that can be used for determining the equilibrium shapes of surfaces of liquids with specified volumes constrained by rigid boundaries. With this method, the element space variables defining the equilibrium surface are expanded in terms of parametric interpolation functions, which are designed such that all of the boundary conditions and the volume (integral) constraint are automatically satisfied during every iteration of the numerical optimization algorithm. The method presents an advantage over other methods in that there is no need to modify the performance index by including the use of a Lagrange multiplier or penalty factor. The results obtained in this study proved to be in good agreement with those obtained experimentally and with other methods.

ACKNOWLEDGMENTS

This research was carried out with funds provided by the Ford Motor Company and Rockwell Automation.

APPENDIX A. NOMENCALTURE

a	liquid/air interface area
a^*	wetted area
a_{xy}	projection of a on xy plane
c	'pressure parameter'
E_{g}	gravitational energy
E_{p}	total potential energy
E_{s}	free surface energy
E_{w}	wetting energy
$\tilde{E}$	$(x_{,\xi})^2 + (y_{,\xi})^2 + (z_{,\xi})^2$
$f(x, y),\ g(x, y),\ h(x, y)$	prescribed functions of z, $z_{,x}$, $z_{,y}$ on Γ
$\tilde{F}$	$x_{,\xi}x_{,\eta} + y_{,\xi}y_{,\eta} + z_{,\xi}z_{,\eta}$
g	gravitational constant
$\tilde{G}$	$(x_{,\eta})^2 + (y_{,\eta})^2 + (z_{,\eta})^2$
J	Jacobian $= \begin{vmatrix} x^e_{,\xi} & x^e_{,\eta} \\ y^e_{,\xi} & y^e_{,\eta} \end{vmatrix}$
m	number of elements used to define the capillary surface
m^*	number of elements used to define the wetted surface
$\bar{r}^e$	space vector with components $\{x^e, y^e, z^e\}$
$\bar{r}^e_0$	space vector with components $\{x^e_0, y^e_0, z^e_0\}$
$\bar{r}^e_{,\xi}$	derivatives of $\bar{r}^e$ with respect to ξ
$\bar{r}^e_{,\eta}$	derivatives of $\bar{r}^e$ with respect to η
V_0	prescribed volume of liquid
x, y, z	modified Cartesian co-ordinates

x_0, y_0, z_0	Cartesian co-ordinates
$\bar{X}^e$	elemental nodal co-ordinate vector

Greek letters

β	$\cos(\theta)$
$\delta(\xi, \eta)$	interpolation function
$\phi_i(\xi, \eta)$	interpolation functions
γ	surface tension constant for liquid/air interface
ρ	liquid density
θ	angle between solid/liquid interface
ξ, η	parametric co-ordinates
Γ	liquid/solid boundary

APPENDIX B. ELEMENT INTERPOLATION FUNCTIONS

$$\phi_1 = (1-\eta)(2\xi^3 - 3\xi^2 + 0.5\xi + 0.5) + (1-\xi)(2\eta^3 - 3\eta^2 + 0.5\eta + 0.5)$$

$$\phi_2 = \eta(2\xi^3 - 3\xi^2 + \xi) + (1-\xi)(-2\eta^3 + 3\eta^2)$$

$$\phi_3 = (1-\eta)(-2\xi^3 + 3\xi^2) + \xi(2\eta^3 - 3\eta^2 + \eta)$$

$$\phi_4 = \eta(-2\xi^3 + 3\xi^2 - 0.5\xi) + \xi(-2\eta^3 + 3\eta^2 - 0.5\eta)$$

$$\phi_5 = (1-\eta)(\xi^3 - 2\xi^2 + \xi)$$

$$\phi_6 = \eta(\xi^3 - 2\xi^2 - \xi)$$

$$\phi_7 = (1-\eta)(\xi^3 - \xi^2)$$

$$\varphi_8 = \eta(\xi^3 - \xi^2)$$

$$\phi_9 = (1-\xi)(\eta^3 - 2\eta^2 + \eta)$$

$$\phi_{10} = (1-\xi)(\eta^3 - \eta^2)$$

$$\phi_{11} = \xi(\eta^3 - 2\eta^2 + \eta) \quad \text{and} \quad \phi_{12} = \xi(\eta^3 - \eta^2)$$

REFERENCES

1. Laplace PS. *Traite de Mechanique*. Celeste: Paris, 1829.
2. Concus P, Finn R (eds). Variational methods for free surface interfaces. In *Proceedings*, *Vallombrosa Center*, *Menlo Park*, *CA*, *1985*. Springer: New York, 1987.
3. Finn R. *Equilibrium Capillary Surfaces*. Springer: New York, 1986.
4. Greenspan D. On approximating extremals of functions, part 1: the method and examples for boundary value problems. *ICC Bulletins* 1965; **4**: 99–120.
5. Greenspan D. On approximating extremals of functions, part 2: theory and generalizations related to boundary value problems for nonlinear differential equations. *International Journal of Engineering Science* 1967; **5**: 571–588.
6. Concus P. Numerical solution of the minimal surface equation. *Mathematics of Computations* 1967; **21**: 340–350.
7. Hinata M, Masaaki S, Takeshi K. Numerical solution of Plateau's problem. *Mathematics of Computation* 1974; **28**(125): 45–61.
8. Wager HJ. A contribution to the numerical approximation of minimal surfaces. *Computing* 1977; **19**: 35–58.
9. Horning U, Mittelmann H. A finite element method for capillary surfaces with volume constraints. *Journal of Computational Physics* 1990; **87**: 26–136.
10. Racz LM, Szekely J. Determination of equilibrium shapes and optimal volumes of solder droplets in the assembly of surface mounted integrated circuits. *Transactions of the Iron and Steel Institute of Japan International* 2000; **33**(2).
11. Lee TS, Choi TP, Yoo CD. Finite element modeling of three-dimensional solder joint geometry in SMT. *Advances in Electronic Packaging ASME-EEVP* 1995; **10**(2): 1031–1041.
12. Nigro NJ, Zhou J, Heinrich S, Elkouh A, Fournelle R, Lee P. Parametric finite element method for predicting shapes of three dimensional solder joints. *Journal of Electronic Packaging* 1996; **118**: 142–147.
13. Nigro NJ, Heinrigh SM, Elkouh AF, Zou X, Fournelle RA, Lee PS. Finite element method for predicting equilibrium shape of solder joints. *Journal of Electronic Packaging* 1993; **115**(2): 141–146.
14. Arora JS. *Introduction to Optimum Design*. McGraw-Hill: New York, 1989.
15. Hooke R, Jeeves TA. Direct search solution of numerical and statistical problems. *Journal of the Association of Computer Machanics* 1962; **8**(2): 212.

